1 **A unified framework to quantify demographic buffering in natural populations**
2 A manuscript in preparation for submission to ECOLOGY LETTERS
3 Type of article: METHOD
4
5 Gabriel Silva Santos [1,2*], Samuel J L Gascoigne[3*], André Tavares Corrêa Dias[4], Maja Kajin
6 [3,5**♦], Roberto Salguero-Gómez[3♦]
7
8 1 National Institute of the Atlantic Forest (INMA), 29650-000, Santa Teresa, Espírito Santo,
9 Brazil. ssantos.gabriel@gmail.com
10 2 Department of Ecology, Graduate Program in Ecology and Evolution, Rio de Janeiro
11 State University, 524 São Francisco Xavier Street, 20550-900, Maracanã, Rio de Janeiro,
12 Brazil
13 3 Department of Biology, University of Oxford, South Parks Road, OX1 3RB, Oxford, UK.
14 samuel.gascoigne@pmb.ox.ac.uk, rob.salguero@biology.ox.ac.uk,
15 maja.kajin@biology.ox.ac.uk
16 4 Department of Ecology, Institute of Biology, Universidade Federal do Rio de Janeiro,
17 Avenida Carlos Chagas Filho 373, 21941-590 Rio de Janeiro, RJ, Brazil. atcdias@gmail.com
18 5 Department of Biology, Biotechnical Faculty, University of Ljubljana, Večna pot 111, 1000
19 Ljubljana, Slovenia
20
21 [*]Shared first authorship
22 [**]Corresponding author
23 [♦]Shared senior authorship
24
34
35 RUNNING TITLE: Demographic buffering framework (32/45 characters)
36
37 KEYWORDS: COMADRE Animal Matrix Database, elasticity, life-history evolution,
38 natural selection, second-order derivative, sensitivity, stochasticity, variance.
39
40 NUMBER OF WORDS: Abstract – 143/150 words, main text (excluding abstract,
41 acknowledgements, references, table, and figure legends) – 4966/5000 words
42
43 NUMBER OF REFERENCES: 60
44
45 NUMBER OF TABLES: 1 (in Supplementary Material)
46
47 NUMBER OF FIGURES: 3
48
49

50   **Abstract** (143/150 words)

51   The Demographic Buffering Hypothesis (DBH) predicts that natural selection reduces the

52   temporal fluctuations in demographic processes (such as survival, development, and

53   reproduction), due to their negative impacts on population dynamics. However, a

54   comprehensive approach that allows for the examination of demographic buffering patterns

55   across multiple species is still lacking. Here, we propose a three-step framework aimed at

56   quantifying demographic buffering. Firstly, we categorize species along a continuum of

57   variance based on the sums of stochastic elasticities. Secondly, we examine the linear

58   selection gradients, followed by the examination of nonlinear selection gradients as the third

59   step. With these three steps, our framework overcomes existing limitations of conventional

60   approaches to quantify demographic buffering, allows for multi-species comparisons, and

61   offers insight into the evolutionary forces that shape demographic buffering. We apply this

62   framework to mammal species and discuss both the advantages and potential of our

63   framework.

64

65

66

Environmental stochasticity shapes organisms' life histories (Bonsall & Klug 2011). Nonetheless, how organisms will cope with the increasing variation in environmental conditions (Boyce *et al.* 2006; Morris *et al.* 2008) remains an intriguing ecological and evolutionary question (Sutherland *et al.* 2013). Evolutionary demography provides diverse explanations for how evolutionary processes shape demographic responses to environmental stochasticity (Charlesworth 1994; Healy *et al.* 2019; Hilde *et al.* 2020; Pfister 1998; Tuljapurkar *et al.* 2009). The long-term stochastic population growth rate, expressed as the geometric mean of annual growth rates (Tuljapurkar 1982), forms the basis of the Demographic Buffering Hypothesis (DBH) (Morris & Doak 2004; Pélabon *et al.* 2020).

Increasing the geometric mean of λ corresponds to a rise in the long-term stochastic population growth rate (λ_s, hereafter). Conversely, higher variance in λ reduces λ_s (Morris & Doak 2004; Tuljapurkar 1982), impacting population persistence. The DBH predicts that life histories are under selection pressure to minimise the negative impacts of environmental variation by constraining the temporal variance of those demographic processes (*e.g.*, survival, development, reproduction) to which population growth rate (*i.e.*, fitness) is most sensitive to (Gaillard & Yoccoz 2003; Pfister 1998). The *demographic pattern* operating the DBH, *i.e.,* demographic buffering, describes the selection-driven constraint on the temporal variance of the most impacting demographic processes for the population growth rate (Hilde *et al.* 2020; Morris & Doak 2004; Pfister 1998). Here, we focus on the latter - on the emerging pattern of demographic buffering in different animal life histories – rather than on the DBH itself.

A unified approach to unambiguously quantify demographic buffering is still missing. Indeed, identifying demographic buffering remains challenging (Doak *et al.* 2005; Morris & Doak 2004) for several reasons, one of them being different interpretation of results from correlational analyses (*e.g.*, as in Pfister, 1998). Some authors rank species' life histories on a

92   continuum from buffered to labile using the correlation coefficient (Spearman's correlation

93   ρ), where negative values indicate buffering (McDonald *et al.* 2017). Alternatively, the

94   absence of statistical support for buffering may suggest a preference for demographic

95   variance to track environmental conditions, known as the Demographic Lability Hypothesis

96   (DLH) (Hilde *et al.* 2020; Jäkäläniemi *et al.* 2013; Koons *et al.* 2009; Reed & Slade 2012).

97   However, increased temporal variance alone is not enough to constitute demographic lability;

98   it must also result in significant changes in the mean value of the demographic process (Le

99   Coeur *et al.* 2022).

100 Another obstacle to achieving generalization across species' populations regarding

101 demographic buffering is the typical hierarchical level of examination. Some studies focus on

102 characteristics drawn from the *entire population model* (*between-populations level*)

103 (McDonald *et al.* 2017; Reed & Slade 2012). At this level, a life history is considered

104 demographically buffered if key demographic processes have low temporal variance (Le

105 Coeur *et al.* 2022; Hilde *et al.* 2020; Morris & Doak 2004; Pfister 1998). However, to fully

106 grasp how and why demographic buffering occurs, and how patterns might change in

107 response to the environment, we must also consider characteristics at the level of separate

108 *components of population model* (*within-populations level*). Within a population, one

109 demographic process may be buffered while another may be labile (Barraquand & Yoccoz

110 2013; Jongejans *et al.* 2010; Koons *et al.* 2009). Thus far, studies have focused on either one

111 of the hierarchical levels, however, for a mechanistic understanding of how environmental

112 stochasticity shapes life histories, both between- and within-population levels need to be

113 addressed at the same time.

114 The complexity of examining the underlying mechanisms of demographic buffering

115 presents additional challenge. Evidence suggests buffering in both long-lived (Doak *et al.*

116 2005; Gaillard & Yoccoz 2003; McDonald *et al.* 2017; Pfister 1998; Rotella *et al.* 2012), and

117   short-lived species (Ferreira *et al.* 2013; Pfister 1998; Reed & Slade 2012). However, these

118   patterns alone do not fully reveal how life histories are shaped by natural selection. First-

119   order effects, such as elasticities, show how variation in demographic processes affects

120   population growth rate, while second-order effects reveal sensitivity to autocorrelation

121   (Tuljapurkar 1990). Integrating both allows a better understanding of fitness function

122   behaviour near local maxima and minima.

123   In linear relationships between fitness and demographic processes, second-order

124   derivatives of population growth rate are zero, indicating natural selection acts on mean

125   values (Shyu & Caswell 2014). Nonzero second derivatives suggest nonlinear relationships

126   between fitness and a demographic process, revealing additional aspects of selection on the

127   variances and covariances of demographic processes (Brodie *et al.* 1995; Carslake *et al.*

128   2008; Shyu & Caswell 2014). The sign (>0, =0, <0) of the self-second derivative of λ with

129   respect to demographic processes determines the type of selection. Negative values describe

130   concave (∩-shaped) selection, reducing temporal variance (Caswell 1996, 2001; Shyu &

131   Caswell 2014) and thus, indicating demographic buffering. Positive values indicate convex

132   (∪-shaped) selection, amplifying variance (Caswell 1996, 2001; Shyu & Caswell 2014) and

133   potentially indicating demographic lability (Le Coeur *et al.* 2022; Koons *et al.* 2009). To

134   confirm lability, increased variance must shift the mean value of a demographic process,

135   outweighing its negative effect on population growth rate (Le Coeur *et al.* 2022).

136   The diverse demographic strategies across species result from evolutionary processes

137   shaping variance in demographic processes over time. Integrating demographic buffering into

138   the context of linear and nonlinear selection enables quantification of the evolutionary forces

139   driving these patterns, shedding light on how environmental variability shapes existing and

140   novel strategies. Despite this, a unified approach to characterize demographic buffering

141   signatures remains lacking.

142   Here, we introduce a framework to quantify demographic buffering, offering insight

143 into temporal variance patterns affected by environmental stochasticity. This framework

144 involves categorizing species or populations along a variance continuum based on the degree

145 of natural selection buffering key demographic processes, with three steps incorporating well-

146 known methods applied to stage-structured demographic data (*e.g.*, matrix population models

147 [Caswell 2001]; integral projection models [(Easterling et al. 2000]). First, species or

148 populations are positioned on the continuum to assess cumulative effects of variance in

149 demographic processes on population growth rate. Second, linear selection forces within the

150 life cycle of each species or population are investigated at the within-populations level. Third,

151 non-linear selection forces within the life cycle are explored at the within-populations level.

152 These steps provide quantitative evidence of demographic buffering occurrence. Lastly,

153 further analyses are proposed to identify demographic lability.

154   To demonstrate the applicability of our framework, we apply it to 40 populations of

155 34 mammal species sourced from the COMADRE database (Salguero-Gómez *et al.* 2016).

156 We showcase how the framework can provide valuable insights into the patterns of

157 demographic buffering across species. The framework offers novel, detailed insights into the

158 selection pressures that act within species' life cycles, thus allowing for a thorough

159 understanding of the evolutionary selection forces that shape the patterns of demographic

160 buffering across species. Beyond providing a quantitative, systematic toolset to quantify

161 buffering through three steps, we have also offered an alternative fourth step that briefly

162 outlines how to evidence lability.

163

164 **A unified framework to assess evidence of demographic buffering**

165 The evidence for demographic buffering has been mainly assessed using Matrix Population

166 Models (MPM; Pfister 1998; Rotella et al. 2012)). However, Integral Projection Models

167   (IPM; Rodríguez-Caro et al. 2020; Wang et al. 2023) can be equally applied for identifying

168   the demographic buffering signatures. Both MPMs and IPMs are stage-structured, discrete-

169   time demographic models (Caswell 2001; Ellner *et al.* 2016). For simplicity, here we focus

170   on MPMs, but note that the same approaches are as equally applicable to IPMs (Doak *et al.*

171   2021; Griffith 2017). Throughout this manuscript, we refer to demographic processes as both

172   matrix entries a_{ij} (*i.e.,* upper-level parameters) and the vital rates that underline the matrix

173   elements (*i.e.,* lower-level parameters), and note that their conversion is straightforward and

174   described elsewhere (Franco & Silvertown 2004). The framework operates on three steps.

175   In the first step of our framework, we calculate the impact of variation in demographic

176   processes on the stochastic growth rate, λ_s, known as stochastic elasticities E_{ij}^S (Haridas &

177   Tuljapurkar 2005) (Figure 1A). This calculation separates the sum of all stochastic elasticities

178   ($\Sigma E_{a_{ij}}^S$) into two components: one for assessing how temporal variance affects λ_s ($\Sigma E_{a_{ij}}^{S^{\sigma}}$), and

179   the other for assessing the impact of mean values of demographic processes on λ_s, ($\Sigma E_{a_{ij}}^{S^{\mu}}$)

180   (Haridas & Tuljapurkar 2005). A higher absolute value of the sum of stochastic elasticity

181   with respect to variance ($\Sigma E_{a_{ij}}^{S^{\sigma}}$), indicates greater sensitivity of λ_s to changes in demographic

182   process variance, suggesting absence of buffering. Conversely, a lower absolute value

183   suggests demographic buffering, where λ_s is less sensitive to such perturbations (Haridas &

184   Tuljapurkar 2005; Tuljapurkar *et al.* 2003) (Fig. 1A). This step places species or populations

185   along a continuum based on variance in demographic processes, with unconstrained variance

186   on the left (possibly unbuffered) and constrained variance on the right (possibly buffered).

187   However, unconstrained variance does not necessarily imply demographic lability, defined as

188   an increase in *mean value* of a demographic process in response to improved environmental

189   conditions (Le Coeur *et al.* 2022). By examining $\Sigma E_{a_{ij}}^{S^{\sigma}}$, we can assess changes in the

190   contribution of demographic process variance to λ_s, while mean values remain unchanged.

191   Although this step provides insight into how environmental variation affects λ_s, it does not

192   consider covariances between demographic processes and serial correlations, which are

193   important for fully diagnosing buffering (Haridas & Tuljapurkar 2005). Instead, our approach

194   focuses on second derivatives of population growth rate with respect to demographic

195   processes to elucidate selection's impact on variance (step 3, below).

196   Steps 2 and 3 of the framework delve into within-population analysis. After step 1

197   positions species or populations along the variance continuum for λ_s, each life cycle

198   undergoes scrutiny. Step 2 (Fig. 1B) involves calculating the partial derivatives of λ_t

199   concerning all matrix elements of the MPM. This step reveals how each demographic process

200   influences λ_t. In step 3, one evaluates nonlinear selection patterns using self-second

201   derivatives of λ_t for each demographic process (Fig. 1C). This step unveils potential nonlinear

202   selection pressures on demographic processes, crucial for understanding their evolutionary

203   dynamics. Failure to consider these evolutionary processes in step 1 may lead to

204   misinterpretation of patterns (*e.g.*, Lawler et al. 2009).

205   Steps 2 and 3 of the framework analyse averaged selection pressures over time

206   periods. They offer insights into how perturbations in demographic processes affect λ_t,

207   obtained by averaging sequential Matrix Population Models (MPMs) across the study

208   duration. Therefore, they enhance our understanding of selection pressures' role in shaping

209   demographic patterns across various species.

210   In step 3, it is important to note that the importance of demographic processes shifts

211   with changing environments (Stearns 1992). This dynamic sensitivity of λ_t to specific

212   processes (Kroon *et al.* 2000), indicated by self-second derivatives, helps pinpoint which

213   processes are most likely to induce changes. For instance, in the hypothetical wolf species

214   (Fig. 1), a decline in reproduction among third age-class individuals (matrix element $a_{1,3}$)

215   would heighten sensitivity to that process. Consequently, with increased environmental

216   variability, the key demographic process might change from remaining in the fourth age class

217   (matrix element $a_{4,4}$, Fig. 1B) to reproduction of the third age-class (matrix element $a_{1,3}$, Fig.

218   1C).

219   Combining the three steps of our framework allows for a quantitative identification of

220   buffering. Steps 2 and 3 offer key insights as to *why* a given species or population is placed

221   on either the buffered or the non-buffered end of the variance continuum. A clear and

222   unequivocal evidence for support towards buffering consists of: (1) a species or population

223   being positioned near the 0 end of the continuum (the right-hand side) in step 1; (2) this

224   species' or populations' life cycle having one or more demographic processes with highest

225   elasticity values in step 2; and (3) the same demographic process displaying the highest

226   elasticity in step 2 with negative self-second derivative values in step 3. In this sense, Figure

227   1B shows that, for the chosen population of a hypothetical wolf species, the most important

228   demographic process is remaining in the fourth stage (MPM element $a_{4,4}$), as this

229   demographic process results in highest elasticity value (Fig. 1B yellow square). However,

230   Fig. 1C reveals that $a_{4,4}$ is under little selection pressure for variance reduction. Thus, there is

231   no clear evidence of buffering from the third step of the framework (*i.e.,* no concave selection

232   forces). This way, the lack of concave selection forces on the key demographic process

233   within wolf's life cycle explains why this species is placed on the left-hand side of the

234   variance continuum (Fig. 1A).

235   Although not our primary goal here, we briefly introduce said step 4. To establish

236   compelling evidence of lability, it is essential to fulfil several further criteria. First, sufficient

237   data across various environments (over time or space) are required to construct reaction

238   norms that depict how a demographic process responds to environmental changes (Koons *et*

239   *al.* 2009; Morris *et al.* 2008), which can be challenging in terms of sufficient and high-quality

240   demographic and environmental data. Second, non-linear relationships between demographic

241   processes and the environment must be established based on the demographic process-

242   environment reaction norms. Lastly, demographic processes where an increase in the mean

243   value has a stronger positive impact on population growth rate than the detrimental effect of

244   increased variance needs to be identified. The latter condition is only met when the

245   demographic process-environment reaction norm takes a convex shape (resembling a "∪"

246   shape), as described by Koons et al. (2009) and Morris et al. (2008). However, a study by

247   Barraquand & Yoccoz (2013) reported diverging results in this regard. Importantly, we note

248   that more likely than previously thought (*e.g.*, Pfister 1998), species do not exist as purely

249   buffering or labile, but that within populations, some vital rates may be buffered, other labile,

250   and others insensitive to the environment (*e.g.*, Doak et al. 2005). Deciphering generality in

251   this likely complex pattern should attract much research attention going forward, in our

252   opinion.

253
254   **Demographic buffering in mammals: a case study using the unified framework**

255   We demonstrate the performance of our framework using 44 MPMs from 34 mammal

256   species. Mammals are of special interest here for two reasons: (1) mammalian life histories

257   have been well studied (Bielby *et al.* 2007; Gillespie 1977; Jones 2011; Stearns 1983); and

258   (2) some of their populations have already been assessed in terms of buffering, particularly

259   for primates (Campos *et al.* 2017; Morris *et al.* 2008, 2011; Reed & Slade 2012; Rotella *et al.*

260   2012). Together, the well-studied life histories and previous information about the occurrence

261   of buffering in mammals provide the necessary information to make accurate predictions and

262   validate the performance of the proposed framework.

263   We used Matrix Population Models from 40 out of 139 studies with mammals

264   available in the COMADRE database v.3.0.0 (Salguero-Gómez *et al.* 2016). These 40

265   populations encompass 34 species from eight taxonomic orders. We included these MPMs in

266   our analyses because they provide values of demographic processes (a_{ij}) for three or more

267   contiguous time periods, thus allowing us to obtain the stochastic elasticity of each a_{ij}.

268   Although we are aware that not all possible temporal variation in demographic processes may

269   have been expressed within this period, we assumed three or more transitions are enough to

270   provide sufficient variation for population comparison. At least three contiguous time periods

271   - a common selection criteria in comparative studies of stochastic demography (Compagnoni

272   *et al.* 2023) - also allowed to test and showcase our framework. Fortunately, several long-

273   lived species, characterized by low variation in their demographic processes, were studied for

274   a long time (*e.g.,* some primates in our dataset have been studied for over 20 years – Morris

275   *et al*. 2011). We removed the populations where either only survival or only reproduction

276   rates were reported, because of the impossibility to calculate the stochastic growth rate. A

277   detailed description of the analysed data and their original sources are available in

278   supplementary material (Supplementary Material, Table S1).

279   *Homo sapiens* was included in our analyses because it is the only mammalian species

280   in which second-order derivatives have been applied (Caswell 1996). Therefore, *Homo*

281   *sapiens* provides an ideal basis for comparisons among species. The data for *Homo sapiens*

282   were gathered from 26 modern populations located in various cities, allowing us to construct

283   a spatiotemporal variance. It is important to note that in this case, we are not working with

284   true temporal variance but rather a variance that encompasses both spatial and temporal

285   aspects.

286   For steps 2 and 3 of our framework, we utilized a subset of 16 populations (including

287   *Homo sapiens*) whose population projection matrices (MPMs) were organized by age. We

288   specifically selected these populations because their life cycles can be summarized by two

289   main demographic processes: survival and contribution to recruitment of new individuals.

290   The contribution to recruitment can be interpreted as either the mean reproductive output for

291   each age class or an approximation thereof, depending on how the matrices are structured

292   (Ebert 1999). One advantage of using such matrices is that they encompass only two types of

293   demographic processes, namely survival and recruitment, eliminating the need to account for

294   multiple transitions between different life stages.

295   To perform the step 1 of our framework and obtain the $\Sigma E_{a_{ij}}^{S^\sigma}$ (and $\Sigma E_{a_{ij}}^{S^\mu}$), we followed

296   Tuljapurkar et al. (2003) and Haridas & Tuljapurkar (2005). To perform step 2 of our

297   framework, we calculated the deterministic elasticities of each demographic process extracted

298   using the *popbio* package. All analyses were performed using R version 3.5.1 (R Core team,

299   2018). Finally, to perform the step 3 of our framework the self-second derivatives were

300   adapted from *demogR* (Jones 2007) following (Caswell 1996) and applied for the mean

301   MPM.

302   *Results*

303   We ranked 40 populations from the 34 identified mammal species according to the

304   cumulative impact of variation in demographic processes on λ_s using the step 1 of our

305   framework (Fig. 2). Additional information (including standard deviations of the elasticity

306   estimates and number of matrices available) is provided in the supplementary material (Table

307   S1). Most of the analysed orders were placed on the low-variance end of the variance

308   continuum (Fig. 2). The smallest contributions of variation in demographic processes (*i.e.,*

309   maximum value of $\Sigma E_{a_{ij}}^{S^\sigma}$, note that $\Sigma E_{a_{ij}}^{S^\sigma}$ ranges from 0 to -1), suggesting more buffered

310   populations, were assigned to Primates: northern muriqui (*Brachyteles hyphoxantus*, $\Sigma E_{a_{ij}}^{S^\sigma} = -$

311    $0.09 \times 10^{-4} \pm 0.12 \times 10^{-4}$) (mean ± standard deviation) (Fig. 2 silhouette a), mountain gorilla

312   (*Gorilla beringhei*, $\Sigma E_{a_{ij}}^{S^\sigma} = -0.24 \times 10^{-4} \pm 0.08 \times 10^{-4}$) (Fig. 2 silhouette b), followed by the

313   blue monkey (*Cercopithecus mitis*, $\Sigma E_{a_{ij}}^{S^\sigma} = -0.63 \times 10^{-4} \pm 0.06 \times 10^{-4}$) (Fig. 2 silhouette c).

314   The first non-primate species placed near the low-variance end of the continuum was the

315   Columbian ground squirrel (*Urocitellus columbianus*, Rodentia, $\Sigma E_{a_{ij}}^{S^\sigma} = -0.003 \pm 0.002$) (Fig.

316   2 silhouette d). The species with the highest contribution of variation in demographic

317   processes placed at the high-variance end of the continuum was the stoat (*Mustela erminea*,

318   Carnivora, $\Sigma E_{a_{ij}}^{S^\sigma} = -0.35 \pm 0.02$) (Fig. 2 silhouette e). All the 14 primate populations

319   displayed potential evidence of buffering, occupying the right-hand side of the variance

320   continuum, with the exception of the Patas monkey (*Erythrocebus patas*, Primates, $\Sigma E_{a_{ij}}^{S^\sigma} = -$

321   0.05 ± 0.03) (Fig. 2 silhouette f). The snowshoe hare (*Lepus americanus*, Lagomorpha, $\Sigma E_{a_{ij}}^{S^\sigma}$

322   $= -0.29 \pm 0.16$) (Fig. 2 silhouette g) and the Bush rat (*Rattus fuscipes*, Rodentia, $\Sigma E_{a_{ij}}^{S^\sigma} = -0.25$

323   ± 0.03) (Fig. 2 silhouette h) appear on the high-variance end of the continuum.

324   As predicted for the steps 2 and 3, we could not observe a clear pattern in support of

325   buffering. This finding means that the demographic processes with the highest elasticity

326   values failed to display strongly negative self-second derivatives (Fig. 3). Particularly for

327   majority of primates - with the lack or minor temporal variation in demographic processes -

328   demographic processes with high elasticities had positive values for the self-second

329   derivatives (indicated by yellow squares with white dots in Fig. 3). Examples of primate

330   species exhibiting high elasticities and positive values for the self-second derivatives and

331   include northern muriqui (*Brachyteles hypoxanthus*), mountain gorilla (*Gorilla beringei*),

332   white-faced capuchin monkey (*Cebus capucinus*), rhesus monkey (*Macaca mulatta*), blue

333   monkey (*Cercopithecus mitis*), Verreaux's sifaka (*Propithecus verreauxi*) and olive baboon

334   (*Papio cynocephalus*) (Fig. 3). This implies that the key demographic processes influencing

335   λ_t are not subject to selective pressure for reducing their temporal variability. However, even

336   though the primates were positioned closer to the low-variance end of the continuum in step

337   1, the evidence from steps 2 and 3 does not support the occurrence of buffering in the most

338   influential demographic processes.

339   The killer whale showed similar controversy between step 1 and steps 2-3 results as

340   most primates. In step 1, the killer whale was positioned at the buffered end of the variance

341   continuum (*Orcinus orca*, Cetacea, $\Sigma E^{S^{\sigma}}_{a_{ij}}$ = -0.70 × 10^{-4} ± 1.04 × 10^{-5}) (Fig. 2 silhouette not

342   shown). However, steps 2 and 3 show that the three demographic processes in killer whale

343   life cycle with highest elasticity values (matrix elements $a_{2,2}$, $a_{3,3}$ and $a_{4,4}$) are not under

344   selection pressures for reducing their temporal variance, but the opposite (depicted by yellow

345   and green squares with white dots, Fig. 3).

346   The only primate species exhibiting evidence of buffering in steps 2 and 3 was

347   human. In human, demographic parameters representing survival from first to second age

348   class (matrix element $a_{2,1}$) displayed high elasticities and negative self-second derivatives

349   (depicted as yellow squares with black dots in Fig. 3). Evidence supporting buffering was

350   also found in the Columbian ground squirrel (*Urocitellus columbianus*), where, similar to

351   humans, survival from the first to the second age class (matrix element $a_{2,1}$) showed

352   indications of selection acting to reduce $a_{2,1}$variance. Accordingly, the Columbian ground

353   squirrel was positioned close to the buffered end of the variance continuum in step 1. Hence,

354   the Columbian ground squirrel was the sole species with consistent evidence of buffering

355   across all three steps of the framework.

356   The Soay sheep (*Ovis aries*) was the species furthest from the buffered end of the

357   variance continuum that enabled to perform steps 2 and 3. For the Soay sheep, remaining in

358   the third age class (matrix element $a_{3,3}$) has the major influence on λ_t and is under selection

359   pressure to have its variance increased. The latter characteristics reveal potential conditions

360   for lability even though the species is placed closer to the buffered end of the variance

361   continuum.

362   Steps 2 and 3 illustrate the importance of examining buffering evidence on the within-

363   populations level. These two steps of the framework identify the simultaneous acting of

364   concave and convex selection on different demographic processes within a single life cycle.

365   In polar bear (*Ursus maritimus*), the key demographic process (matrix element $a_{4,4}$) is under

366   convex selection, as depicted by a yellow square with a white dot in Fig. 3. However, the

367   demographic process with the second highest elasticity value (matrix element $a_{5,4}$) is under

368   strong concave selection (depicted by a light green square with a black dot in Fig. 3).

369   By adding step 3 to the framework, another important information was accessed. The

370   high absolute values of self-second derivatives (large dots, either black or white, Fig. 3)

371   indicate where the sensitivity of λ_t to demographic parameters is itself prone to environmental

372   changes. For instance, if the value of $a_{5,4}$ for polar bear increased, the sensitivity of λ_t to $a_{5,4}$

373   would decrease because the self-second derivative of $a_{5,4}$ is highly negative (depicted by the

374   largest black dot in polar bear MPM). Vice versa holds for the $a_{4,4}$ demographic process,

375   where an increase in the value of $a_{4,4}$ would increase λ_t's sensitivity to $a_{4,4}$, because the self-

376   second derivative of $a_{5,4}$ is highly positive (depicted by the largest white dot in polar bear

377   MPM). Thus, sensitivities (or equally elasticities) of demographic processes with high

378   absolute values for self-second derivatives can easily change.

379

380   **Discussion**

381   In the Anthropocene, identifying and quantifying mechanisms of species responses to

382   stochastic environments holds crucial importance. This importance is particularly tangible in

383   the context of the unprecedented environmental changes and uncertainties that impact the

384   dynamics and persistence of natural populations (Boyce *et al.* 2006). Correlational

385   demographic analysis, whereby the importance of demographic processes and their temporal

386   variability is examined (Pfister 1998), has attempted to identify how species may buffer

387 against the negative effects of environmental stochasticity. However, these widely used

388 approaches have important limitations (see Introduction and Hilde *et al*. 2020). One

389 significant limitation is the issue of measurement scale concerning demographic processes

390 (Hilde *et al*. 2020; Morris & Doak 2004). Demographic processes, such as birth rates, death

391 rates, immigration, and emigration, operate at various temporal and spatial scales. The choice

392 of scale at which these processes are measured can impact the outcomes of correlational

393 demographic analysis (Bjørkvoll *et al.* 2016). Our novel framework overcomes said

394 limitations by providing a rigorous approach to quantify demographic buffering (Hilde et al.

395 2020; Pfister 1998).

396 　　　Evidencing demographic buffering is not straightforward. Indeed, through the

397 analysis of stochastic population growth rate (λ_s) in our application of the framework to 44

398 populations of 34 species, we identify the highest density of natural populations near the

399 buffered end of the variance continuum (step 1). However, we show that the same species

400 then fail to exhibit signs of concave (∩-shaped) selection on the key demographic parameters

401 when further analyses are performed averaging the variation across the duration of each study

402 (steps 2 and 3). This finding confirms that placing the species near the buffered end of the

403 variance continuum is *necessary* but not *sufficient* to diagnose demographic buffering.

404 Indeed, buffering occurs when concave selection forces act on the key demographic

405 parameter (Caswell 1996, 2001; Shyu & Caswell 2014).

406 　　　Combining the three steps into a unified framework is of outmost importance. In steps

407 2 and 3 of the framework, we find relatively limited overall evidence of buffering in the

408 examination of our 16 (out of 34 in step 1) studied animal species. Step 3 of our framework

409 reveals that the role of natural selection shaping temporal variation in demographic processes

410 is more complex than expected. Indeed, demographic processes within our study populations

411 are often under a mix of convex and concave selection. This mix of selection patterns was

already suggested by Doak *et al.* (2005). Here, only two out of 16 mammal species revealed

concave selection acting on the key demographic processes (Columbian ground squirrel

[*Urocitellus columbianus*], and humans, [*Homo sapiens sapiens*]). These two species were

also placed near the buffered end of the variance continuum, therefore meeting all the

necessary conditions to diagnose buffering. However, finding 12.5% (two out of 16) species

that meet the criteria for demographic buffering is not in concordance with previous studies.

Evidence of buffering has been reported across 22 ungulate species (Gaillard & Yoccoz

2003). In the one ungulate we examined, the moose (*Alces alces*), we find only partial

support for buffering in adult survival, since this species is placed near the buffered end of

the variance continuum in step 1 but does not show concave selection pressures on adult

survival in step 2/3, as would be necessary to confirm the occurrence of buffering.

It is worth noting that a varying number of matrices per species were employed,

ranging from 1 to 21, with an average of 8.1 matrices per species (as shown in Table S1).

Naturally, having a greater number of matrices is preferred in such analyses. Furthermore,

while the size of matrices (matrix dimensions) does not directly bias the results of our

framework in any way – since steps 2 and 3 are shown for all the demographic processes

independent of matrix dimension – potential implications of varying matrix dimensions

should be further investigated in the future.

Our overall findings reveal varying levels of support for the notion that adult survival

in long-lived species tends to be buffered. Indeed, (Gaillard *et al.* 1998) found that adult

female survival varied considerably less than juvenile survival in large herbivores. This

finding was also supported by further studies in ungulates and small rodents (Gaillard &

Yoccoz 2003), turtles (Heppell 1998), vertebrates and plants (Pfister 1998), and more

recently across nine (out of 73) species of plants (McDonald *et al.* 2017).

When placing our study species along a variance continuum (step 1), primates tend to be located on the buffered end. However, most primates displayed convex –instead of the expected concave– selection on adult survival. Similar results, where the key demographic process failed to display constrained temporal variability, have been reported for long-lived seabirds (Doherty *et al.* 2004). One explanation for the unexpected convex selection on adult survival involves trade-offs, as suggested by (Doak *et al.* 2005). When two demographic parameters are negatively correlated, the variance of population growth rate (λ) can be increased or decreased (Compagnoni *et al.* 2016; Evans & Holsinger 2012). The well-established trade-off between survival and fecundity (Roff & Fairbairn 2007; Stearns 1992) might explain the observed deviation of our results. Because variation in primate recruitment is already constrained by physiological limitations (Campos *et al.* 2017), when adult survival and recruitment are engaged in a trade-off, this trade-off might lead to our unexpected result. Correlations among demographic processes (positive and negative) inherently influence the biological limits of variance (Haridas & Tuljapurkar, 2005). This is because the magnitude of variation in a particular demographic process is constrained by (the variation of) other demographic processes that exert an influence on it. Not surprisingly, correlations among demographic processes have been shown to be strongly subjected to ecological factors (Fay *et al.* 2022). Here, future studies may benefit from deeper insights via cross-second derivatives (Caswell 1996, 2001) to investigate correlations among demographic processes.

Examining the drivers of demographic buffering has become an important piece of the ecological and evolutionary puzzle of demography. As such, quantifying buffering can help us better predict population responses to environmental variability, climate change, and direct anthropogenic disturbances (Boyce *et al.* 2006; McDonald *et al.* 2017; Pfister 1998; Vázquez *et al.* 2017). By setting demographic buffering into a broader and integrated framework, we hope to enhance comprehension and prediction of the implications of heightened

461 environmental stochasticity on the evolution of life history traits. This understanding is

462 crucial in mitigating the risk of extinction for the most vulnerable species.

463

470

Data availability

472 The demographic data used in this paper are open-access and available in the COMADRE

473 Animal Matrix Database (https://compadre-db.org/Data/Comadre). A list of the studies and

474 species used here is available in Supplementary Material (Table S1). The data and code

475 supporting the results can be accessed here:

476 https://github.com/SamuelGascoigne/Demographic_buffering_unified_framework.

477

478 **References**

479 Barraquand, F. & Yoccoz, N.G. (2013). When can environmental variability benefit
480   population growth? Counterintuitive effects of nonlinearities in vital rates. *Theor Popul*
481   *Biol*, 89, 1–11.

482 Bielby, J., Mace, G.M., Bininda-Emonds, O.R.P., Cardillo, M., Gittleman, J.L., Jones, K.E.,
483   *et al.* (2007). The Fast-Slow Continuum in Mammalian Life History: An Empirical
484   Reevaluation. *Am Nat*, 169, 748–757.

485 Bjørkvoll, E., Lee, A.M., Grøtan, V., Saether, B.-E., Stien, A., Engen, S., *et al.* (2016).
486   Demographic buffering of life histories? Implications of the choice of measurement
487   scale. *Ecology*, 97, 40–47.

488 Bonsall, M.B. & Klug, H. (2011). The evolution of parental care in stochastic environments.
489   *J Evol Biol*, 24, 645–655.

Boyce, M.S., Haridas, C. V., Lee, C.T., Boggs, C.L., Bruna, E.M., Coulson, T., *et al.* (2006). Demography in an increasingly variable world. *Trends Ecol Evol*, 21, 141–148.

Brodie, E.I., Moore, A. & Janzen, F. (1995). Visualizing and quantifying natural selection. *Trends Ecol Evol*, 10, 313–318.

Campos, F.A., Morris, W.F., Alberts, S.C., Altmann, J., Brockman, D.K., Cords, M., *et al.* (2017). Does climate variability influence the demography of wild primates? Evidence from long-term life-history data in seven species. *Glob Chang Biol*, 23, 4907–4921.

Carslake, D., Townley, S. & Hodgson, D.J. (2008). Nonlinearity in eigenvalue-perturbation curves of simulated population projection matrices. *Theor Popul Biol*, 73, 498–505.

Caswell, H. (1996). Second Derivatives of Population Growth Rate: Calculation and Applications. *Ecology*, 77, 870–879.

Caswell, H. (2001). *Matrix Population Models: Construction, Analysis, and Interpretation*. Sinauer Associates Inc. Publishers, Sunderland, Massachusetts, USA.

Charlesworth, B. (1994). *Evolution in age-structured populations*. second edi. Cambridge University Press.

Le Coeur, C., Yoccoz, N.G., Salguero-Gómez, R. & Vindenes, Y. (2022). Life history adaptations to fluctuating environments: Combined effects of demographic buffering and lability. *Ecol Lett*, 1–13.

Compagnoni, A., Bibian, A.J., Ochocki, B.M., Rogers, H.S., Schultz, E.L., Sneck, M.E., *et al.* (2016). The effect of demographic correlations on the stochastic population dynamics of perennial plants. *Ecol Monogr*, 86, 480–494.

Compagnoni, A., Evers, S. & Knight, T. (2023). Spatial replication can best advance our understanding of population responses to climate. *bioRxiv*, https://doi.org/10.1101/2022.06.24.497542.

Doak, D.F., Morris, W.F., Pfister, C., Kendall, B.E. & Bruna, E.M. (2005). Correctly Estimating How Environmental Stochasticity Influences Fitness and Population Growth. *Am Nat*, 166, E14–E21.

Doak, D.F., Waddle, E., Langendorf, R.E., Louthan, A.M., Isabelle Chardon, N., Dibner, R.R., *et al.* (2021). A critical comparison of integral projection and matrix projection models for demographic analysis. *Ecol Monogr*, 91, e01447.

Doherty, P.F., Schreiber, E.A., Nichols, J.D., Hines, J.E., Link, W.A., Schenk, G.A., *et al.* (2004). Testing life history predictions in a long-lived seabird: A population matrix approach with improved parameter estimation. *Oikos*, 105, 606–618.

Easterling, M.R., Ellner, S.P. & Dixon, P.M. (2000). Size-Specific Sensitivity: Applying a New Structured Population Model. *Ecology*, 81, 694–708.

Ebert, T. (1999). *Plant and animal populations: Methods in demography*. Academis Press, San Diego, CA, USA.

527 Ellner, S.P., Childs, D.Z. & Rees, M. (2016). *Data-driven Modelling of Structured*
528   *Populations. A practical guide to the Integral Projection Model.* Lecture Notes on
529   Mathematical Modelling in the Life Sciences. Springer International Publishing, Cham.

530 Evans, M.E.K. & Holsinger, K.E. (2012). Estimating covariation between vital rates : A
531   simulation study of connected vs . separate generalized linear mixed models (GLMMs).
532   *Theor Popul Biol*, 82, 299–306.

533 Fay, R., Hamel, S., van de Pol, M., Gaillard, J.M., Yoccoz, N.G., Acker, P., *et al.* (2022).
534   Temporal correlations among demographic parameters are ubiquitous but highly
535   variable across species. *Ecol Lett*, 25, 1640–1654.

536 Ferreira, M., Kajin, M., Vieira, M., Zangrandi, P., Cerqueira, R. & Gentile, R. (2013). Life
537   history of a neotropical marsupial: Evaluating potential contributions of survival and
538   reproduction to population growth rate. *Mamm Biol*, 78, 406–411.

539 Franco, M. & Silvertown, J. (2004). A comparative demography of plants based upon
540   elasticities of vital rates. *Ecology*, 85, 531–538.

541 Gaillard, J.M., Festa-Bianchet, M. & Yoccoz, N.G. (1998). Population dynamics of large
542   herbivores: Variable recruitment with constant adult survival. *Trends Ecol Evol*, 13, 58–
543   63.

544 Gaillard, J.-M. & Yoccoz, N. (2003). Temporal Variation in Survival of Mammals: a Case of
545   Environmental Canalization? *Ecology*, 84, 3294–3306.

546 Gillespie, J.H. (1977). Natural Selection for Variances in Offspring Numbers: A New
547   Evolutionary Principle. *Am Nat*, 111, 1010–1014.

548 Griffith, A.B. (2017). Perturbation approaches for integral projection models. *Oikos*, 126,
549   1675–1686.

550 Haridas, C. V. & Tuljapurkar, S. (2005). Elasticities in variable environments: Properties and
551   implications. *American Naturalist*, 166, 481–495.

552 Healy, K., Ezard, T.H.G., Jones, O.R., Salguero-Gómez, R. & Buckley, Y.M. (2019). Animal
553   life history is shaped by the pace of life and the distribution of age-specific mortality and
554   reproduction. *Nat Ecol Evol*, 3, 1217–1224.

555 Heppell, S.S. (1998). Application of Life-History Theory and Population Model Analysis to
556   Turtle Conservation. *Copeia*, 1998, 367.

557 Hilde, C.H., Gamelon, M., Sæther, B.-E., Gaillard, J.-M., Yoccoz, N.G. & Pélabon, C.
558   (2020). The Demographic Buffering Hypothesis: Evidence and Challenges. *Trends Ecol*
559   *Evol*, 35, 523–538.

560 Jäkäläniemi, A., Ramula, S. & Tuomi, J. (2013). Variability of important vital rates
561   challenges the demographic buffering hypothesis. *Evol Ecol*, 27, 533–545.

562 Jones, J.H. (2007). demogR: A Package for the Construction and Analysis of Age-structured
563   Demographic Models in R. *J Stat Softw*, 22, 1–28.

Jones, J.H. (2011). Primates and the evolution of long, slow life histories. *Current Biology*, 21, R708–R717.

Jongejans, E., De Kroon, H., Tuljapurkar, S. & Shea, K. (2010). Plant populations track rather than buffer climate fluctuations. *Ecol Lett*, 13, 736–743.

Koons, D.N., Pavard, S., Baudisch, A. & Jessica E. Metcalf, C. (2009). Is life-history buffering or lability adaptive in stochastic environments? *Oikos*, 118, 972–980.

Kroon, H. De, Groenendael, J. Van & Ehrlen, J. (2000). Elasticities: A review of methods and model limitations. *Ecology*, 81, 607–618.

Lawler, R.R., Caswell, H., Richard, A.F., Ratsirarson, J., Dewar, R.E. & Schwartz, M. (2009). Demography of Verreaux's sifaka in a stochastic rainfall environment. *Oecologia*, 161, 491–504.

McDonald, J.L., Franco, M., Townley, S., Ezard, T.H.G., Jelbert, K. & Hodgson, D.J. (2017). Divergent demographic strategies of plants in variable environments. *Nat Ecol Evol*, 1, 0029.

Morris, W.F., Altmann, J., Brockman, D.K., Cords, M., Fedigan, L.M., Pusey, A.E., *et al.* (2011). Low Demographic Variability in Wild Primate Populations: Fitness Impacts of Variation, Covariation, and Serial Correlation in Vital Rates. *Am Nat*, 177, E14–E28.

Morris, W.F. & Doak, D.F. (2004). Buffering of Life Histories against Environmental Stochasticity: Accounting for a Spurious Correlation between the Variabilities of Vital Rates and Their Contributions to Fitness. *Am Nat*, 163, 579–590.

Morris, W.F., Pfister, C.A., Tuljapurkar, S., Haridas, C. V., Boggs, C.L., Boyce, M.S., *et al.* (2008). Longevity can buffer plant and animal populations against changing climatic variability. *Ecology*, 89, 19–25.

Pélabon, C., Hilde, C.H., Einum, S. & Gamelon, M. (2020). On the use of the coefficient of variation to quantify and compare trait variation. *Evol Lett*, 4, 180–188.

Pfister, C. (1998). Patterns of variance in stage-structured populations: Evolutionary predictions and ecological implications. *Proceedings of the National Academy of Sciences*, 95, 213–218.

Reed, A.W. & Slade, N.A. (2012). Buffering and plasticity in vital rates of oldfield rodents. *Journal of Animal Ecology*, 81, 953–959.
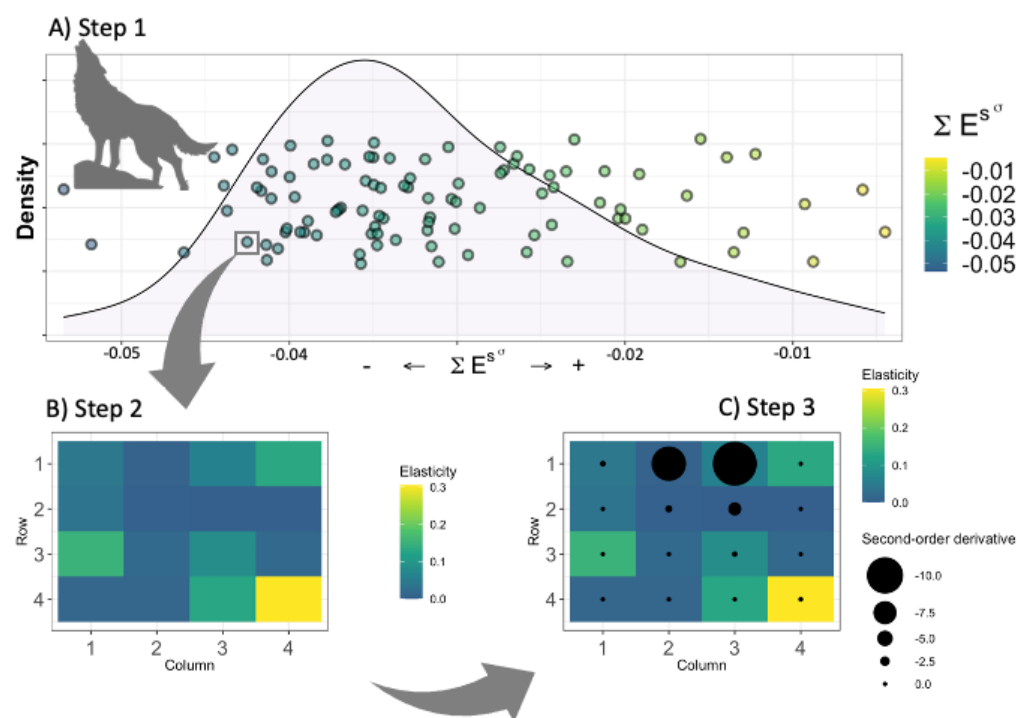
Rodríguez-Caro, R.C., Capdevila, P., Graciá, E., Barbosa, J.M., Giménez, A. & Salguero-Gómez, R. (2020). The demographic buffering strategy has a threshold of effectiveness to increases in environmental stochasticity. *bioRxiv*, 1–41.

Roff, D.A. & Fairbairn, D.J. (2007). The evolution of trade-offs: Where are we? *J Evol Biol*, 20, 433–447.

Rotella, J.J., Link, W.A., Chambert, T., Stauffer, G.E. & Garrott, R.A. (2012). Evaluating the demographic buffering hypothesis with vital rates estimated for Weddell seals from 30 years of mark – recapture data, 162–173.
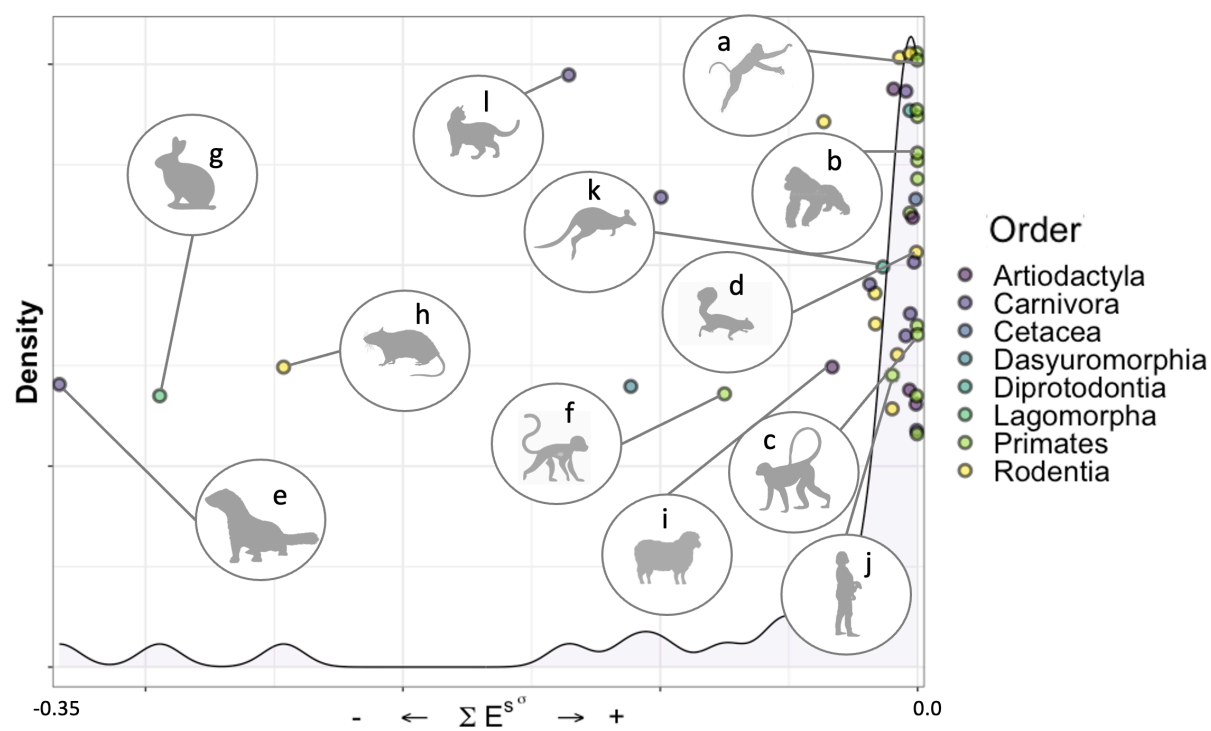
602 Salguero-Gómez, R., Jones, O.R., Archer, C.R., Bein, C., de Buhr, H., Farack, C., *et al.*
603   (2016). COMADRE: A global data base of animal demography. *Journal of Animal*
604   *Ecology*, 85, 371–384.

605 Shyu, E. & Caswell, H. (2014). Calculating second derivatives of population growth rates for
606   ecology and evolution. *Methods Ecol Evol*, 5, 473–482.

607 Stearns, S. (1992). *The Evolution of Life Histories*. Oxford University Press, New York,
608   USA.

609 Stearns, S.C. (1983). The Influence of Size and Phylogeny on Patterns of Covariation among
610   Life-History Traits in the Mammals. *Oikos*, 41, 173.

611 Sutherland, W.J., Freckleton, R.P., Godfray, H.C.J., Beissinger, S.R., Benton, T., Cameron,
612   D.D., *et al.* (2013). Identification of 100 fundamental ecological questions. *Journal of*
613   *Ecology*, 101, 58–67.

614 Tuljapurkar, S. (1990). Population Dynamics in Variable Environments. In: *Lecture notes in*
615   *Biomathematics*, Lecture Notes in Biomathematics (ed. Levin, S.). Springer Berlin
616   Heidelberg.

617 Tuljapurkar, S., Gaillard, J.-M. & Coulson, T. (2009). From stochastic environments to life
618   histories and back. *Philosophical Transactions of the Royal Society B: Biological*
619   *Sciences*, 364, 1499–1509.

620 Tuljapurkar, S., Horvitz, C.C. & Pascarella, J.B. (2003). The Many Growth Rates and
621   Elasticities of Populations in Random Environments. *Am Nat*, 162, 489–502.

622 Tuljapurkar, S.D. (1982). Population dynamics in variable environments. III. Evolutionary
623   dynamics of r-selection. *Theor Popul Biol*, 21, 141–165.

624 Vázquez, D.P., Gianoli, E., Morris, W.F. & Bozinovic, F. (2017). Ecological and
625   evolutionary impacts of changing climatic variability. *Biological Reviews*, 92, 22–42.

626 Wang, J., Yang, X., Silva Santos, G., Ning, H., Li, T., Zhao, W., *et al.* (2023). Flexible
627   demographic strategies promote the population persistence of a pioneer conifer tree
628   (Pinus massoniana) in ecological restoration. *For Ecol Manage*, 529, 120727.
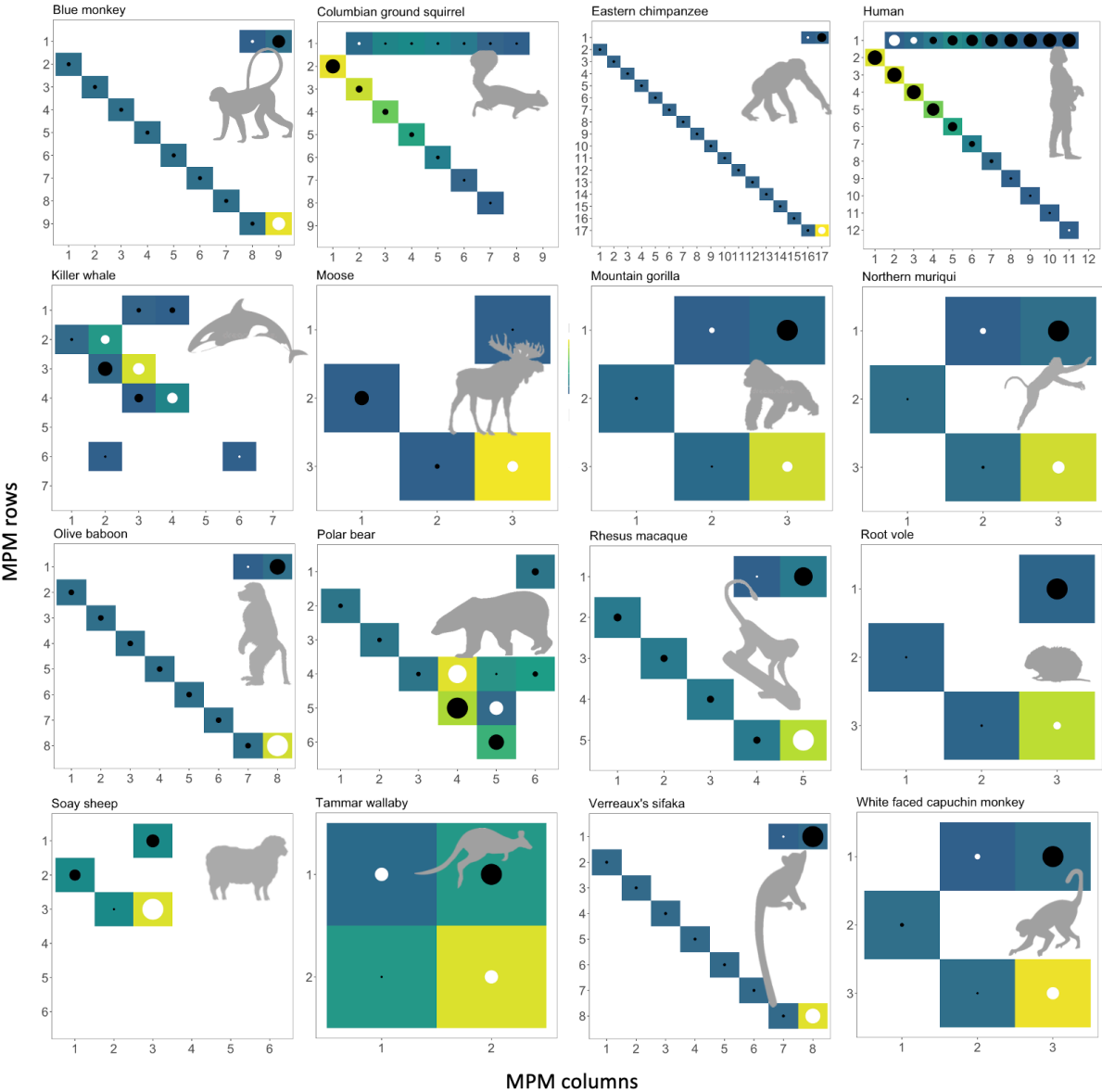
629

630

631 **Figure 1**

632

Figure 2

Figure 3

Figure legends

Figure 1. A three-step framework proposed to: Step 1 - allocate species and/or populations

on a variance continuum (plot A, dots representing 50 hypothetical species). The variance

continuum operates at the between-populations level (see text) and is represented by

partitioning the sum of all the stochastic elasticities ($\Sigma E^{S}_{a_{ij}}$) into two compounds: i) sums of

stochastic elasticities with respect to the variance ($\Sigma E^{S^{\sigma}}_{a_{ij}}$), and ii) sums of stochastic

elasticities with respect to the mean ($\Sigma E^{S^{\mu}}_{a_{ij}}$). The first step of our framework shows the

variance compound of the sums of stochastic elasticities forming a continuum where the

right-hand side of the plot represents species (or populations) where a perturbation of

variance in demographic processes results in weak or no impact on λ_s (yellow dots). The

yellow-dotted species (or populations) can be classified as having potentially *buffered life-*

cycles – based on all the demographic processes. The left-hand side of the graph represents

species (or populations) where a perturbation of the variance in demographic processes

results in strong impact on λ_s (blue dots). Thus, the blue-dotted species (or populations) can

be classified as having potentially *unbuffered life cycles* – based on all the demographic

processes. The vertical axis delineates the values of the density distribution function,

indicating the number of species/populations at each value of $\Sigma E^{S^{\sigma}}_{a_{ij}}$. The placement of data

points (species/populations) along the horizontal axis corresponds to their calculated values

of $\Sigma E^{S^{\sigma}}_{a_{ij}}$ and is arranged linearly, while the breadth along the y-axis is solely for improved

visual comprehension. Step 2 - Access the linear selection pressures for individual species or

populations at within-species level (see text) (plot B). Step 2 displays the elasticities of the

deterministic population growth rate (λ_t) for a hypothetical population of wolf and reveals the

linear selection gradients, and which demographic processes are the most influential for λ_t.

Step 3 - Access the nonlinear selection pressures at the within-species level (see text) (plot

665   C). In the third step self-second derivatives for the corresponding demographic processes

666   from step 2 are displayed.

667

668   **Figure 2**. Results for step 1 of our framework showing the sum of stochastic elasticities with

669   respect to the variance $\Sigma E^{S^\sigma}_{a_{ij}}$. The closer the $\Sigma E^{S^\sigma}_{a_{ij}}$ is to zero, the weaker the impact of

670   variation in demographic processes on λ_s. The 40 populations from 34 species of mammals

671   from the COMADRE database are ranked into the variance continuum from potentially

672   buffered (right-hand side) to less buffered (left-hand side), since any variation in

673   demographic processes would strongly impact λ_s. Colors represent different taxonomic orders

674   with Primates occupying the right-hand side. Silhouettes: a) *Brachyteles hyphoxantus*, b)

675   *Gorilla beringhei*, c) *Cercopithecus mitis*, d) *Urocitellus columbianus,* e) *Mustela erminea*, f)

676   *Erythrocebus patas*, g) *Lepus americanus*, h) *Rattus fuscipes*, i) *Ovis aries*, j) *Homo sapiens*,

677   k) *Macropus eugenii*, and l) *Felis catus*. The vertical axis delineates the values of the density

678   distribution function, indicating the number of species/populations at each value of $\Sigma E^{S^\sigma}_{a_{ij}}$.

679   The placement of data points (species/populations) along the horizontal axis corresponds to

680   their calculated values of $\Sigma E^{S^\sigma}_{a_{ij}}$ and is arranged linearly, while the breadth along the y-axis is

681   solely for improved visual comprehension.

682

683   **Figure 3:** Results from steps 2 and 3 of the proposed framework (see Fig. 2B, C). The 16

684   plots represent populations where the MPMs built by ages were available in the COMADRE

685   database (see text). The color scale represents elasticity values for each of the demographic

686   processes in the MPM, where yellow represents high and blue low elasticity values. No color

687   means elasticity=0. Because the aim of step 2 is to identify the most impacting demographic

688   process within each species' life cycle (the within-populations level, see text) - not to

689   compare the elasticity values among species - each plot has its own scale (see end of legend).

690   The black dots represent negative self-second derivatives of λ_t - thus concave selection - and

691   the white dots represent positive self-second derivatives of λ_t - thus convex selection. The dot

692   sizes are scaled by the absolute value of self-second derivatives, where the smaller the dot,

693   the closer a self-second derivative is to 0, indicting weak or no nonlinearity. Large dots

694   indicate strong nonlinear selection forces. Scales ($E_{min-max}$=elasticity minimum and maximum

695   value, $SSD_{min-max}$=self-second derivative minimum and maximum value): Blue monkey $E_{min-max}$=0.00-0.52, $SSD_{min-max}$=-1.25-1.27; Columbian ground squirrel: $E_{min-max}$=0.00-0.23,

696

697    $SSD_{min-max}$=-1.48-0.01; Eastern chimpanzee: $E_{min-max}$=0.00-0.60, $SSD_{min-max}$=-4.39-2.59;

698   Human: $E_{min-max}$=0.00-0.18, $SSD_{min-max}$=-0.15-0.08; Killer whale: $E_{min-max}$=0.00-0.55,

699    $SSD_{min-max}$=-5.72-3.43; Moose: $E_{min-max}$=0.00-0.55, $SSD_{min-max}$=-0.66-0.36; Mountain gorilla:

700    $E_{min-max}$=0.00-0.81, $SSD_{min-max}$=-1.46-0.28; Northern muriqui: $E_{min-max}$=0.00-0.72, $SSD_{min-max}$=-1.17-0.35; Olive baboon: $E_{min-max}$=0.00-0.54, $SSD_{min-max}$=-0.57-1.13; Polar bear: $E_{min-max}$=0.00-0.26, $SSD_{min-max}$=-0.73-0.54; Rhesus macaque: $E_{min-max}$=0.00-0.51, $SSD_{min-max}$=-0.54-0.71; Root vole: $E_{min-max}$=0.00-0.86, $SSD_{min-max}$=-2.54-0.22; Soay sheep: $E_{min-max}$=0.00-0.56, $SSD_{min-max}$=-0.22-0.40; Tammar wallaby: $E_{min-max}$=0.00-0.55, $SSD_{min-max}$=-0.64-0.34;

701

702

703

704

705   White faced capuchin monkey: $E_{min-max}$=0.00-0.66, $SSD_{min-max}$=-2.66-1.21.

706

707   **Supplementary material – Data available in COMADRE Version 2.0.1 and results from**
708   **Step 1 of the framework**

709   **Table S1.** The metadata used in step 1 of our framework and the respective results presented

710   in the main text. The first four columns represent the information from where Matrix

711   Populations Models (MPMs) were extract precisely as presented in COMADRE 2.0.1.

712   Column titles differ from the database as "SpeciesAuthorComadre" is equivalent to

713   "SpeciesAuthor" and "SpeciesName" is equivalent to "SpeciesAccepted" in COMADRE

714   2.0.1. The remaining columns present the results of step 1, where we present the raw values

715   of $\Sigma E^{S^\mu}_{a_{ij}}$ and $\Sigma E^{S^\sigma}_{a_{ij}}$, their respective standard deviation, the stochastic population growth rate

716   λ_s, and the number of available matrices (# matrices). For ByAge, "TRUE" was assigned for

717   MPMs built by age or "FALSE" if otherwise.

SpeciesAuthorComadre	SpeciesName	CommonName	Order	ΣE
Homo_sapiens_subsp._sapiens	*Homo sapiens sapiens*	Human	Primates	1.003
Alces_alces	*Alces alces*	Moose	Artiodactyla	1.001
Antechinus_agilis	*Antechinus agilis*	Agile antechinus	Dasyuromorphia	1.111
Brachyteles_hypoxanthus	*Brachyteles hypoxanthus*	Northern muriqui	Primates	1.000
Callospermophilus_lateralis	*Callospermophilus lateralis*	Golden-mantled ground squirrel	Rodentia	1.054
Cebus_capucinus	*Cebus capucinus*	White faced capuchin monkey	Primates	1.000
Cercopithecus_mitis	*Cercopithecus mitis*	Blue monkey	Primates	1.000
Eumetopias_jubatus	*Eumetopias jubatus*	Northern sea lion; Steller sea lion	Carnivora	1.005
Felis_catus	*Felis catus*	Feral cat	Carnivora	1.136
Gorilla_beringei	*Gorilla beringei*	Mountain gorilla	Primates	1.000
Hippocamelus_bisulcus	*Hippocamelus bisulcus*	Huemul deer	Artiodactyla	1.002
Lepus_americanus	*Lepus americanus*	Snowshoe hare	Lagomorpha	1.294
Lycaon_pictus	*Lycaon pictus*	African wild dog	Carnivora	1.100
Macaca_mulatta_3	*Macaca mulatta*	Rhesus macaque	Primates	1.000
Macropus_eugenii	*Macropus eugenii*	Tammar wallaby	Diprotodontia	1.013
Marmota_flaviventris_2	*Marmota flaviventris*	Yellow-bellied marmot	Rodentia	1.007
Marmota_flaviventris_3	*Marmota flaviventris*	Yellow-bellied marmot	Rodentia	1.008
Microtus_oeconomus	*Microtus oeconomus*	Root vole	Rodentia	1.000
Mustela_erminea	*Mustela erminea*	Stoat	Carnivora	1.334
Orcinus_orca_2	*Orcinus orca*	Killer whale	Cetacea	1.001
Ovis_aries_2	*Ovis aries*	Soay sheep	Artiodactyla	1.033
Pan_troglodytes_subsp._schweinfurthii	*Pan troglodytes*	Eastern chimpanzee	Primates	1.000
Papio_cynocephalus	*Papio cynocephalus*	Olive baboon	Primates	1.000
Peromyscus_maniculatus_2	*Peromyscus maniculatus*	Deer mouse	Rodentia	1.010
Phocarctos_hookeri	*Phocarctos hookeri*	New Zealand sea lion	Carnivora	1.005
Propithecus_verreauxi	*Propithecus verreauxi*	Verreaux's sifaka	Primates	1.000

Puma_concolor_8	*Puma concolor*	Cougar	Carnivora	NA
Rattus_fuscipes	*Rattus fuscipes*	Bush rat	Rodentia	1.246
Spermophilus_armatus	*Urocitellus armatus*	Uinta ground squirrel	Rodentia	1.016
Spermophilus_armatus_2	*Urocitellus armatus*	Uinta ground squirrel	Rodentia	1.017
Spermophilus_columbianus	*Urocitellus columbianus*	Columbian ground squirrel	Rodentia	1.036
Spermophilus_columbianus_3	*Urocitellus columbianus*	Columbian ground squirrel	Rodentia	1.003
Ursus_americanus_subsp._floridanus	*Ursus americanus*	Florida black bear	Carnivora	1.003
Ursus_arctos_subsp._horribilis_5	*Ursus arctos*	Grizzly bear	Carnivora	1.001
Ursus_maritimus_2	*Ursus maritimus*	Polar bear	Carnivora	1.019
Brachyteles_hypoxanthus_2	*Brachyteles hypoxanthus*	Northern muriqui	Primates	1.000
Cebus_capucinus_2	*Cebus capucinus*	WhiteNAfaced capuchin monkey	Primates	1.000
Chlorocebus_aethiops_2	*Chlorocebus aethiops*	Vervet	Primates	1.075
Erythrocebus_patas	*Erythrocebus patas*	Patas monkey	Primates	1.051
Gorilla_beringei_subsp._beringei	*Gorilla beringei*	Mountain gorilla	Primates	1.000

718

719